Impact of Gaussian Transformation on Cloud Cover Data Assimilation for Historical Weather Reconstruction

Xiaoxing Wang[1,1], Kinya Toride[2,2], and Kei Yoshimura[2,2]

[1]Graduate School of Frontier Sciences, The University of Tokyo
[2]University of Tokyo

November 30, 2022

Abstract

Old descriptive diaries are important sources of daily weather conditions before modern instrumental measurements became available. A previous study demonstrated the potential of reconstructing historical weather at high temporal resolution by assimilating cloud cover converted from descriptive diaries. However, cloud cover often exhibits a non-Gaussian distribution, which violates a basic assumption of most data assimilation schemes. In this study, we applied a Gaussian transformation (GT) approach for cloud cover data assimilation and conducted observing system simulation experiments (OSSEs) using 15 randomly selected observation points over Japan. We performed experiments to assimilate cloud cover with large observational errors using the Global Spectral Model (GSM) and a local ensemble transform Kalman filter (LETKF). Without GT, temperature and zonal and meridional wind exhibited deterioration compared to the experiment assimilating no observations. By contrast, the 2-month root mean square error (RMSE) of zonal wind, meridional wind, temperature, and specific humidity at mid-troposphere were improved by 8.7%, 5.1%, 4.2%, and 1.4%, respectively, through GT. Among two-dimensional variables, the 2-month RMSE of total cloud cover, surface pressure, rainfall, and downward solar radiation were improved by 2.2%, 5.2%, 27.6%, and 4.3%, respectively. We further demonstrated that the effect of GT was more pronounced on clear days. Our results show the potential of GT in high-resolution historical weather reconstruction using old descriptive diaries.

Impact of Gaussian Transformation on Cloud Cover Data Assimilation for Historical Weather Reconstruction

Xiaoxing Wang[1], Kinya Toride[2,3], and Kei Yoshimura[2,4]

[1] Graduate School of Frontier Sciences, The University of Tokyo, Kashiwa, Chiba, Japan

[2] Institute of Industrial Science, The University of Tokyo, Kashiwa, Chiba, Japan

[3] Department of Atmospheric Sciences, University of Washington, Seattle, WA, USA

[4] Earth Observation Research Center, Japan Aerospace Exploration Agency, Japan

Corresponding author: Xiaoxing Wang (wangxx@iis.u-tokyo.ac.jp)

Key Points:

- This is the first study to assimilate cloud cover using Gaussian transformation for historical weather reconstruction
- Assimilating Gaussian-transformed cloud cover improved cloud cover and other atmospheric variables by improving error covariance structure
- Gaussian transformation effects were more pronounced on clear days

Abstract

Old descriptive diaries are important sources of daily weather conditions before modern instrumental measurements became available. A previous study demonstrated the potential of reconstructing historical weather at high temporal resolution by assimilating cloud cover converted from descriptive diaries. However, cloud cover often exhibits a non-Gaussian distribution, which violates a basic assumption of most data assimilation schemes. In this study, we applied a Gaussian transformation (GT) approach for cloud cover data assimilation and conducted observing system simulation experiments (OSSEs) using 15 randomly selected observation points over Japan. We performed experiments to assimilate cloud cover with large observational errors using the Global Spectral Model (GSM) and a local ensemble transform Kalman filter (LETKF). Without GT, temperature and zonal and meridional wind exhibited deterioration compared to the experiment assimilating no observations. By contrast, the 2-month root mean square error (RMSE) of zonal wind, meridional wind, temperature, and specific humidity at mid-troposphere were improved by 8.7%, 5.1%, 4.2%, and 1.4%, respectively, through GT. Among two-dimensional variables, the 2-month RMSE of total cloud cover, surface pressure, rainfall, and downward solar radiation were improved by 2.2%, 5.2%, 27.6%, and 4.3%, respectively. We further demonstrated that the effect of GT was more pronounced on clear days. Our results show the potential of GT in high-resolution historical weather reconstruction using old descriptive diaries.

Plain Language Summary

Climate change greatly affects human society. Learning about past climate helps to predict future changes more accurately. Old diaries provide valuable information about historical weather before modern instrumental measurements became available. Weather information from diaries can be used to reconstruct historical weather by incorporating model simulations. Taking cloud cover as an example, a previous study demonstrated the potential of reconstructing historical weather by diary-based information. However, cloud cover is usually not normally distributed because the probability of no cloud (e.g., sunny days) or frequent clouds (e.g., rainy days) is higher than that of some clouds in practical experience. This violates the normal distribution assumption and indicates some room for improvement. Our results showed that transforming cloud cover distribution into a normal distribution could

improve all atmospheric variables in the model (e.g., wind speed and temperature). In particular, precipitation could be improved by 27%. We demonstrated the critical role of the transformation in a non-normally distributed variable when combining with models and showed the potential of diary-based weather information for actual weather reconstruction.

1 Introduction

Studying historical climate is crucial for understanding Earth systems because it provides a reference for predicting future climate change. However, only a few meteorological observations date back to the early 19th century, and these reflect weather conditions at only a local scale (McElwain & Sweeney, 2007; Pfister *et al*., 2019). Therefore, it is important to reconstruct global-scale climate information recorded before modern instrumental records became available.

Natural proxies provide essential information for reconstructing historical climate variability. For example, speleothems (Proctor *et al*., 2000), tree rings (Shao *et al*., 2005), and lake sediment records (Chu *et al*., 2012) can record climate change information at time scales of 1–10 years. Many studies have reconstructed temperature and precipitation for the past few hundred or even thousands of years at seasonal and annual resolution based on natural proxy data (Chen *et al*., 2015; McDermott, 2004; Striberger *et al*., 2011; Thomas & Briner, 2009; Zhu *et al*., 2008). Although proxy records are beneficial for studying decadal and centennial climate variability, their temporal scales are not suited to elucidating short-term and local variability (Pfister *et al*., 2018), which motivates the reconstruction of daily scale global weather information.

Daily weather data are useful for the accurate characterization of meteorological indices (e.g., drought index) compared to monthly or annual climate data, which can be applied to assess climate impacts (Pfister *et al*., 2020). Old descriptive weather records (e.g., diaries) hold significant potential for daily reconstruction because they precisely record the locations and dates of weather events. Such descriptive historical weather records have been discovered worldwide. Much documentary evidence is available for Asia, Europe, and North America, including China, India, Czech Republic, and Mexico (e.g., Brázdil *et al*., 2019; Domínguez-Castro *et al*., 2019; Mikami, 2008; Mock, 1991; Walsh *et al*., 1999; Zhang *et al*.,

2013). In Japan, the Historical Weather Database (HWDB) stores historical weather diaries, where more than 18 daily observation records are available from the 1750s to 1870s (Yoshimura, 2007). These diaries can be used to reconstruct past climate at high temporal resolution (e.g., Nash *et al*., 2020).

Data assimilation is widely used to reconstruct historical climate because it optimally combines meteorological information with the dynamical constraints of a climate model (Steiger *et al*., 2014). Previous studies have reconstructed annual temperature or precipitation data from proxy records for hundreds to thousands of years using "offline" data assimilation approaches (e.g., Brönnimann *et al*., 2013; Franke *et al*., 2011; Hakim *et al*., 2016). However, as mentioned above, proxy-based reconstruction is limited by low temporal resolution, which is often seasonal at best. By contrast, the Twentieth Century Reanalysis (20CR) project, uses an ensemble Kalman filter data assimilation method to provide a global atmospheric circulation dataset at 6-hourly temporal resolution (Compo *et al*., 2011; Slivinski *et al*., 2019) and covers the period from 1836 to the present. However, the spatial coverage of assimilated surface pressure observations is limited before the 19th century, such that the lack of recovered diaries from many parts of the world imposes additional constraints.

Historical weather reconstruction (as opposed to historical climate reconstruction) using old diaries becomes possible if the descriptive weather information can be incorporated into numerical weather models. Toride *et al*. (2017) proposed converting descriptive Japanese weather records into daily total cloud cover data and investigated the feasibility of reconstructing historical weather using cloud cover assimilation; they showed remarkable improvements in various atmospheric variables by assimilating loosely classified cloud information in idealized experiments with reanalyses, but limitations were reported in ground observation data experiments, demonstrating the challenges of cloud cover assimilation. One possible cause of this issue is that cloud cover often exhibits highly non-Gaussian distribution characteristics, severely violating the basic assumption of normal error statistics in most data assimilation schemes (e.g., Bocquet *et al*., 2010; Tsuyuki & Miyoshi, 2007; Zhang *et al*., 2013).

Previous studies have investigated non-Gaussian issues in precipitation assimilation. Lien *et al*. (2013) transformed precipitation values into a Gaussian distribution based on an empirical cumulative distribution function and indicated that Gaussian transformation (GT)

was beneficial for precipitation assimilation, particularly when observation errors were large. Kotsuki *et al*. (2017) proposed an inverse GT method and demonstrated the usefulness of GT using mock Global Satellite Mapping of Precipitation (GSMaP) data.

In this study, we aimed to improve diary-based historical weather reconstruction using a GT technique. We transformed original cloud cover data into an approximately normal distribution based on the assimilation of an empirical cumulative distribution function within a numerical weather system. To evaluate the performance of the GT, we conducted idealized experiments within an observing system simulation experiment (OSSE) framework assuming Japanese weather records similar to Toride *et al*. (2017) to determine whether GT would improve the impacts of cloud cover assimilation.

2 Methods

2.1 Global Spectral Model

We used the Global Spectral Model (GSM), a numerical atmospheric model initially developed as a seasonal forecasting model by the National Centers for Environmental Prediction (NCEP) (Kanamitsu *et al*., 2002). In this model, variables are represented by a periodic function calculated as the sum of spectral harmonics. The spectral representation calculates the space derivatives strictly, and avoids pole problems and instability due to aliasing in the ideal case (Orszag *et al*., 1970).

The main physics packages in GSM include short- and longwave radiation fluxes (Chou, 1992; Chou & Suarez, 1994), a relaxed Arakawa-Schubert cumulus convective scheme developed by Moorthi and Suarez (1992), non-local vertical diffusion developed by Hong and Pan (1998), mountain drag (Alpert *et al*., 1988), shallow convection (Tiedtke, 1983), and the Noah land surface scheme of Ek *et al*. (2003). We adopted the T62 grid system (about 200 km horizontally) and 28 vertical sigma levels.

2.2 Local ensemble transform Kalman filter (LETKF)

We used the LETKF as the assimilation scheme following Toride *et al*. (2017). For data assimilation, Evensen (1994) developed the ensemble Kalman filter (EnKF), which uses ensembles to estimate the background error covariance. The analyses of EnKF is solved by

the following equations from the original Kalman Filter (Evensen, 2003):

$$X_a = X_b + K(y - H(X_b)) \quad (1)$$

$$K = BH^T(R + HBH^T)^{-1}, \quad (2)$$

where X_a and X_b denote the analysis ensemble and the first guess ensemble (also known as the background ensemble). K represents the Kalman gain, H is the observation operator, y is the observation matrix, and R and B are the observation error covariance and background covariance matrix, respectively.

Following the upgrade of EnKF, Bishop *et al*. (2001) found the transformation matrix in EnKF, known as the ensemble transform Kalman filter (ETKF), to efficiently compute the error covariance. Ott *et al*. (2004) introduced the local ensemble Kalman filter (LEKF), which assimilates observations within a local domain and allows efficient parallel implementation due to independent analyses at each grid point. As the locally applied ETKF, LETKF (Hunt *et al*., 2007) performs simultaneous computation at different grid points through parallel processing and efficiently reduces computational power compared to traditional EnKF.

In this study, the state vector in LETKF (i.e., X_a and X_b) consists of eight atmospheric variables including four 3-dimensional variables at 28 vertical sigma levels (zonal wind, meridional wind, air temperature, and specific humidity) and four two-dimensional variables (total cloud cover, surface pressure, rainfall, and downward solar radiation).

2.3 GT

A Gaussian anamorphosis technique (e.g., Wackernagel, 2003) introduces a transformation algorithm to transform the original variable (y) to a target variable with Gaussian distribution (y_{trans}). In this study, we utilized this algorithm to satisfy the basic assumption of normal error statistics in LETKF. This transformation is performed through the equivalent relationship between two cumulative distribution functions (CDFs) of y and y_{trans}, as follows:

$$y_{trans} = G^{-1}[F(y)], \quad (3)$$

where $F(y)$ is the CDF of the original cloud cover. $F(y)$ is distributed from 0 to 1 by definition, and is determined empirically from original samples, and y_{trans} represents the

transformed variable, which is expected to follow a standard Gaussian distribution with zero mean and unit standard deviation. G^{-1} is the inverse CDF of y_{trans}, such that:

$$G^{-1}(x) = \sqrt{2}\mathrm{erf}^{-1}(2x - 1), \quad (4)$$

where erf^{-1} is the inverse error function.

We used the GSM simulation results to apply this transformation technique. Figure 1 shows the GT procedure for total cloud cover at a model grid point in summer based on 3-year GSM simulation results. The probability density function (PDF) and CDF of the original cloud cover, respectively, are shown in Figure 1a and b, respectively. The original cloud cover CDF was converted into the transformed cloud cover (Figure 1c) using the inverse CDF of a normally distributed variable (G^{-1}). Figure 1d shows the PDF of the transformed cloud cover. Consequently, the original cloud cover, with a numerical range of 0–100, was converted into a rage of –2 to 2, with a distribution similar to the standard Gaussian distribution. The conversion of both the observation and model background fields (i.e., X_b in Eq. (1)) in LETKF follows this one-to-one relationship between the original and transformed values. When conducting GT in the model background field, CDF is calculated grid by grid throughout the observation grid points. At other grid points, the transformed values of a single, specific grid point of Japan are applied globally.

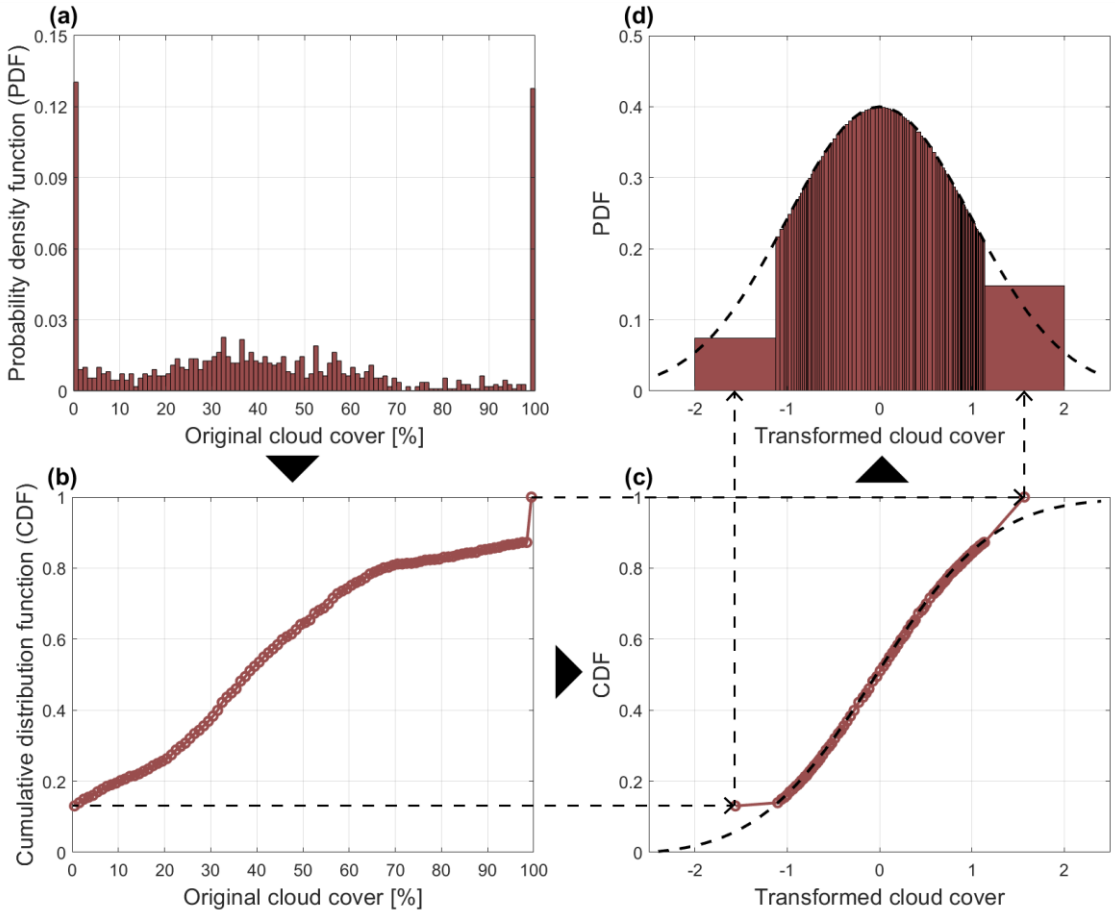

Figure 1. The probability density function (PDF) and cumulative distribution function (CDF) of original cloud cover (a, b) and transformed cloud cover (c, d) at a Global Spectral Model (GSM) grid point including Tokyo during summer (June–August) based on 3-year (2015–2017) GSM simulation results. Gaussian transformation (GT) proceeds from (a) to (b), (c), and (d) as indicated by arrows.

2.4 Experimental design

2.4.1 OSSEs and observation locations

We conducted OSSEs to confirm the feasibility of GT. Compared to the actual experiment, the atmospheric conditions for one OSSE represent a known state simulated by GSM with a 6 h time interval. This known atmospheric state is assumed to represent nature and is used as a reference to evaluate the assimilation analysis results. The "nature" run started from January 1, 2015, with a 1-year spin-up. Cloud cover observations were generated

in the nature run by adding random normally distributed observational errors. We use relatively large observational errors (i.e., standard deviations of 30% and 1 before and after GT, respectively) considering diary-based reconstruction. We performed a control experiment with no observations assimilated (NoDA) and two experimental runs assimilating cloud cover with GT and without GT (NoGT) for the 2-month period from July 1 to August 31, 2017. The initial conditions of the experiments were obtained from the nature run from July 1, 2016, with a 24 h time interval. As a preliminary step toward weather reconstruction based on historical diaries, we selected the vicinity surrounding Japan as the study area. Because diary data collection is ongoing, we randomly selected 15 grid points in Japan and the surrounding area to assimilate cloud cover, including land and marine areas covering 25°–50°N and 125°–150°E (Figure 2).

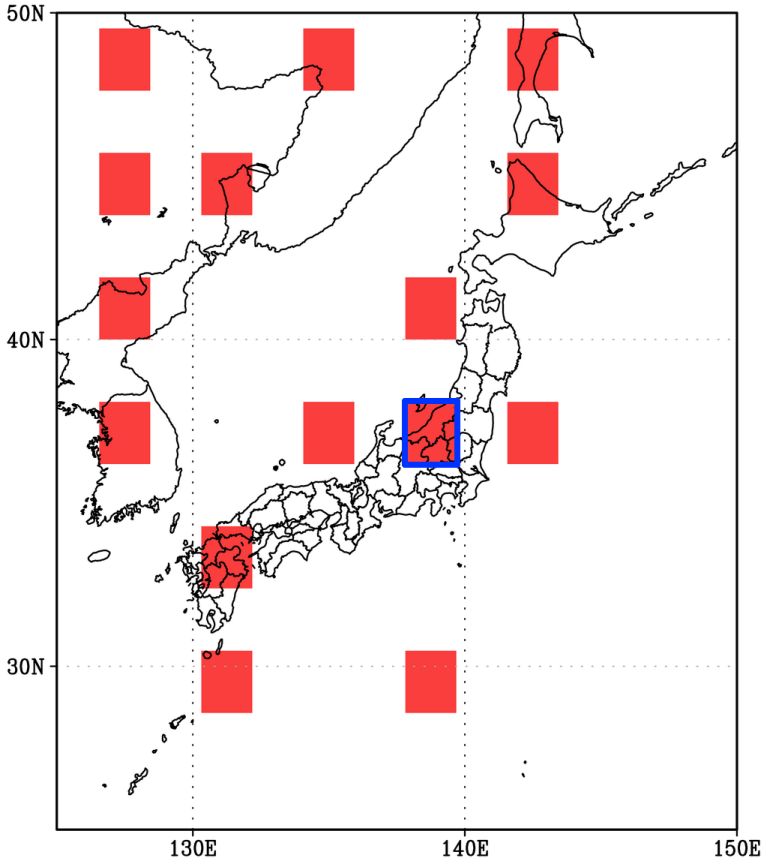

Figure 2. Distribution of observation grid points in observing system simulation experiments (OSSEs). Red boxes indicate computational grid cells with T62 (192 × 94 longitude/latitude) resolution used in the GSM. Blue box indicates a single grid point on Honshu Island, Japan; its results are shown in Figures 6 and S3.

2.4.2 Evaluation factor

Assimilation results were evaluated by comparing the 2-month root mean square error (RMSE) of each experiment and the nature run. We used the RMSE reduction between each experimental run and the control run (NoDA) as the evaluation factor, indicating improvement in cloud cover assimilation. The RMSE reduction was calculated as follows:

$$\frac{RMSE_{NoDA} - RMSE_{NoGT\ or\ GT}}{RMSE_{NoDA}} \times 100\%, \quad (5)$$

where positive values indicate RMSE improvement relative to NoDA and negative values suggest that assimilating cloud cover is inferior even to the control experiment, in which no variables were assimilated.

2.4.3 LETKF ensemble size and covariance inflation method

To balance accuracy and computational cost in assimilation experiments, we conducted pre-experiments using different ensemble member sizes of 20–90. We adopted an ensemble member size of 60 for subsequent experiments, as explained in detail in Text S1 and Figure S1.

The LETKF uses a covariance inflation technique to avoid ensemble spread reduction caused by spurious correlations. We explored different covariance inflation methods and adopted a relaxation-to-prior-spread (RTPS) scheme ($\alpha = 0.5$) (Whitaker & Hamill, 2012) as the covariance inflation method, as explained in detail in Text S2 and Figure S2.

3 Results

3.1 GT improves cloud cover

The horizontal distribution of the 2-month RMSE reduction for cloud cover and for NoDA in the NoGT and GT experiments are shown in Figure 3. Positive values indicate that cloud cover assimilation improved the cloud cover field, and negative values indicate deterioration compared to the control experiment, in which no observations were assimilated. Overall, the cloud cover field over Japan was improved by 2.2% after GT, with 7.24–9.40%

244 increases in regional averaged RMSE reduction.

245 Cloud cover improved markedly near grid points, where cloud cover data were
246 assimilated (Figure 2) in both NoGT and GT, similar to the idealized experiment results
247 reported by Toride *et al*. (2017). This demonstrates the prime importance of spatial coverage
248 in documental records. Large improvements (i.e., RMSE reduction > 10%) were more widely
249 distributed in the GT experiment (Figure 3b), in areas such as the Japan Sea and the Pacific
250 region near northern Japan, indicating that the transformation of both observation and model
251 background covariance into Gaussian distribution brings assimilation results closer to real
252 conditions by accommodating the Gaussian error statistical assumption in the ensemble
253 Kalman filter. Because the whole error covariance structure was improved, the assimilation
254 results also improved, even at grid points without observations, which similarly improved
255 other variables.

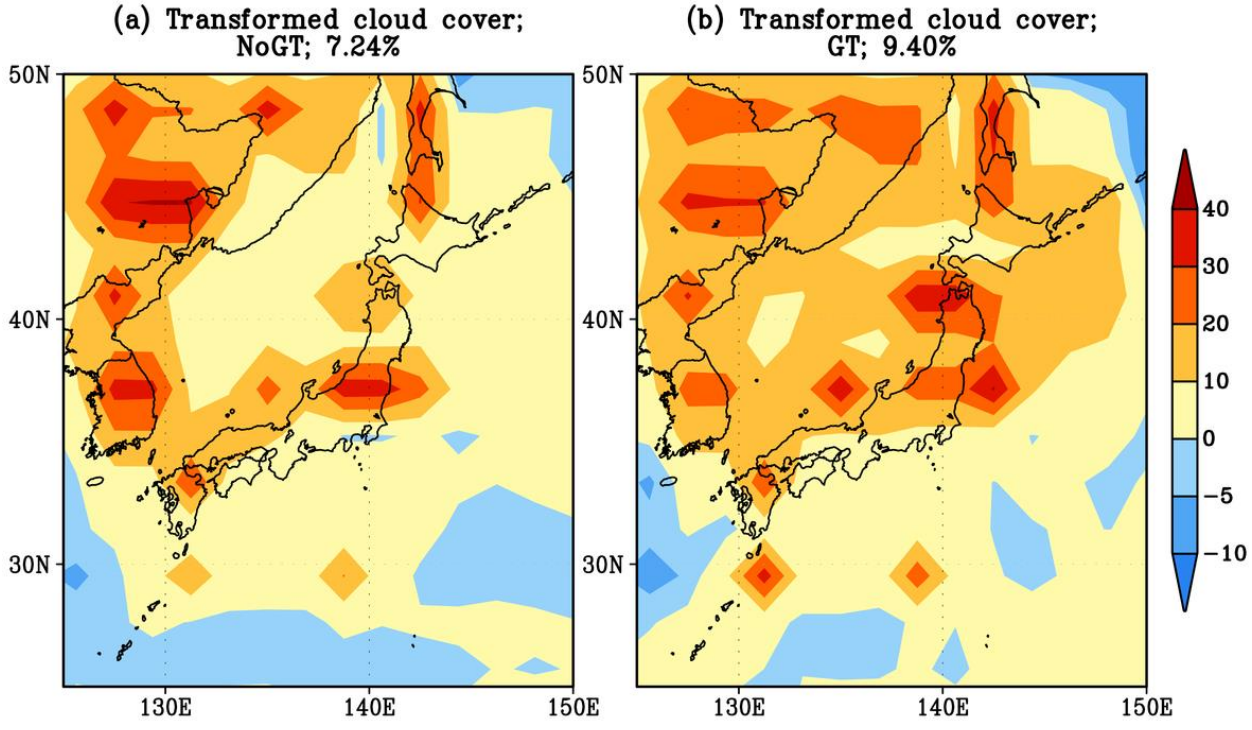

256

257 **Figure 3.** Horizontal distributions of 2-month root mean square error (RMSE) cloud cover
258 reductions in experimental runs (a) without GT (NoGT) and (b) with GT relative to a control
259 experiment with no observations assimilated (NoDA). All cloud cover values were Gaussian
260 transformed for consistency. Percentages are regional averages. Positive values indicate
261 improvement relative to NoDA.

3.2 Improvements in other atmospheric variables by cloud cover GT

We investigated the effects of cloud cover assimilation on other atmospheric variables. The vertical distributions of 2-month RMSE reductions in various variables averaged over Japan are shown in Figure 4. In NoGT, temperature and zonal and meridional wind deteriorated at nearly all heights compared to the control experiment. Specific humidity was improved only within a height range of 200–700 hPa in NoGT. By contrast, GT improved the estimates of all four variables at all heights compared to NoGT. Nearly all variables showed positive RMSE reductions in the GT experiment, confirming that assimilation of the Gaussian-transformed cloud cover improved other variables compared to the control experiment.

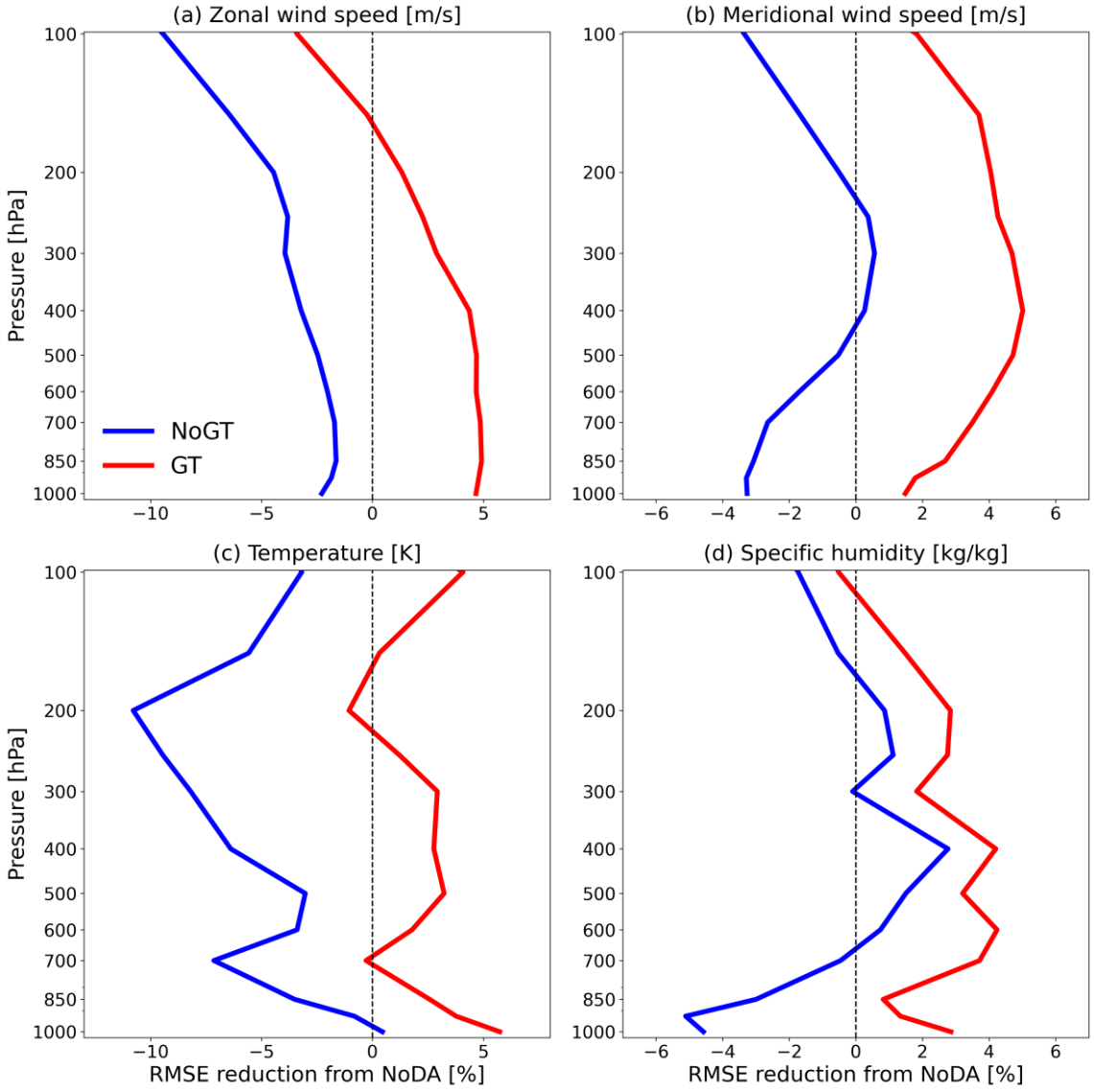

Figure 4. Vertical distributions of 2-month RMSE reductions from NoDA. Blue and red lines indicate RMSE reductions by NoGT and GT, respectively. The results are regional averages of (a) zonal wind, (b) meridional wind, (c) temperature, and (d) specific humidity. Positive values indicate improvement relative to NoDA.

Our subsequent analyses focused on the horizontal distribution of the assimilation impacts. Figure 5 shows the 2-month RMSE reduction for three-dimensional variables at 500 hPa (Figure 5a–h) and surface pressure (Figure 5i,j). GT improved zonal wind, meridional wind, temperature, and specific humidity fields in the mid-troposphere over Japan by 8.7% (regional averaged RMSE reduction increased from –4.37% to 4.33%), 5.1% (–0.90% to

4.22%), 4.2% (–1.68% to 2.50%), and 1.4% (1.73% to 3.16%) compared to NoGT, respectively. It also improved surface pressure estimates by 5.2% (regional averaged RMSE reduction increased from –2.02% to 3.19%).

RMSE reductions for zonal and meridional wind, temperature, and surface pressure were negative in more than half of the regions in the NoGT experiment (Figure 5a, c, e, and i), indicating that worse results were obtained with the assimilation of non-Gaussian distributed variables without correction than without assimilating any observations. GT solved this issue without modifying the EnKF equations. Simulated zonal wind improved considerably except in Kanto, Japan, and the nearby Pacific region (Figure 5b). The meridional wind GT results showed positive values in most areas (Figure 5d).

Although GT led to deterioration in temperature and specific humidity at around 30°N (Figure 5f and h), it was superior to NoGT and NoDA in terms of regional RMSE reduction. Toride *et al*. (2017) showed that 2 m air temperature and specific humidity were improved over central Japan and the ocean to the southeast due to northwestern winds in winter. Our results showed the opposite distribution characteristics because our observational network was different and our assimilation period was summer, when low-pressure systems over the Japanese mainland result in southern winds. Thus, 500 hPa temperature and specific humidity were improved to a greater extent in northern Japan, downstream of the observation grid points.

The effects of GT on improving the surface pressure field was mainly shown over the continental region of Japan (Figure 5j). Although cloud cover GT performance varied among different variables, they generally showed significant positive effects. This result was consistent with those reported in Section 3.1, in that the assimilation of Gaussian-transformed cloud cover improved our estimates of not only cloud cover but also other variables due to improved error covariance structure.

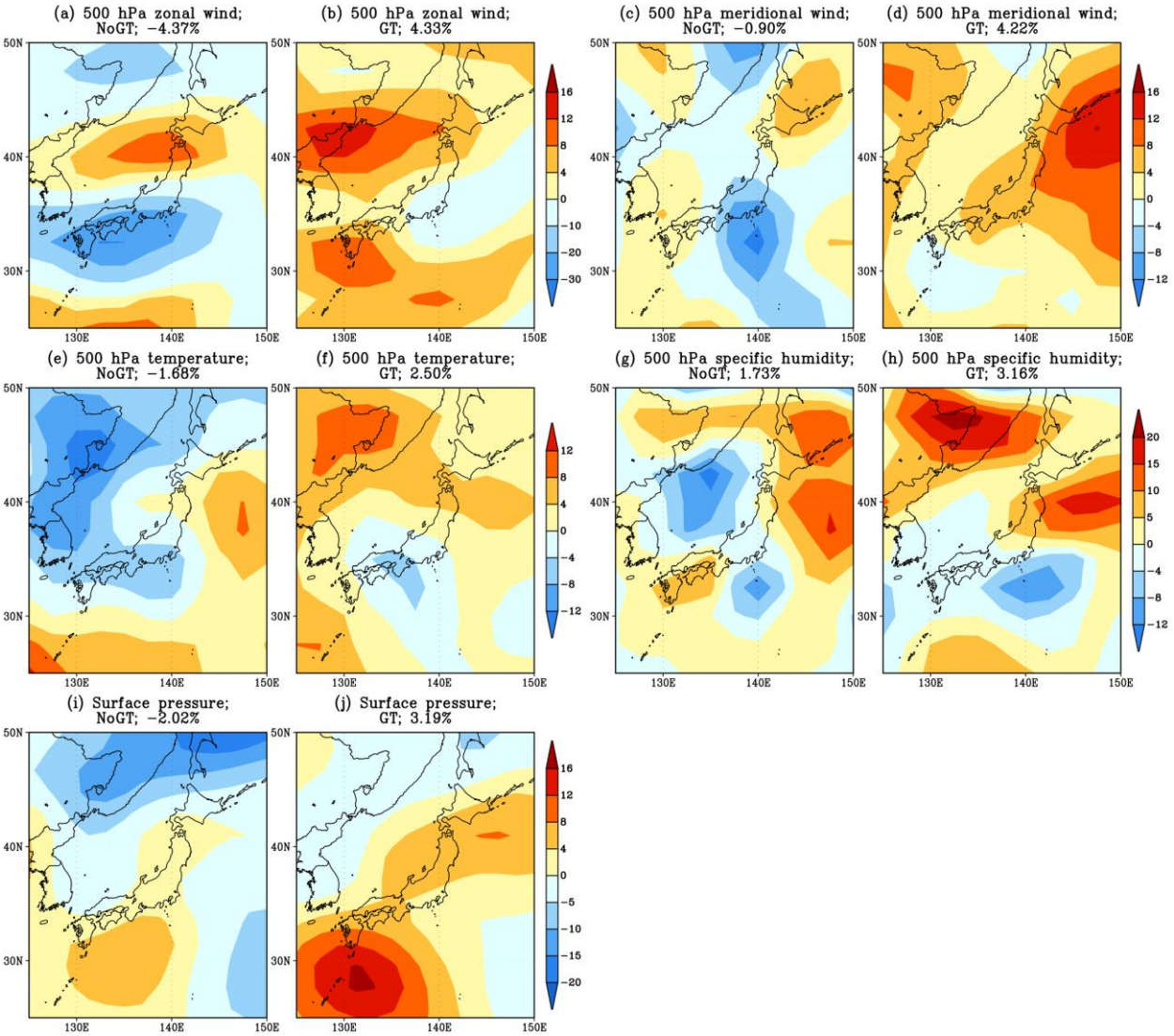

309

310 **Figure 5.** Horizontal distributions of 2-month RMSE reductions of (a, b) zonal wind, (c, d)
311 meridional wind, (e, f) temperature, (g, h) specific humidity, and (i, j) surface pressure. (a–h)
312 Results for 500 hPa. (a, c, e, g, i) and (b, d, f, h, j) are RMSE reductions from NoDA by
313 NoGT and GT, respectively. Percentages are regional averages. Positive values indicate
314 improvement relative to NoDA.

315

316 The effects of GT were also evaluated at a single grid point on Honshu Island, Japan.
317 The 2-month temporal variation in the nature run and the assimilation experiment results are
318 shown in Figure 6, with transformed cloud cover values. At the grid point, NoDA results
319 showed little variability over the 2-month period, whereas the variation amplitude increased
320 after cloud cover was assimilated. In the nature run, cloud cover and the other atmospheric

variables were generally improved when the transformed cloud cover was <–1, such that the original cloud cover was near zero, as shown in Figure 1. For example, the zonal and meridional wind at 500 hPa during periods 1 and 2 (yellow shading, Fig. 6), and surface pressure during periods 2 and 4 of GT were closer to those of the nature run than to those of NoGT. In Figure S3, we show boxplots grouped by transformed cloud cover in the nature run as an example. The RMSE differences between NoGT and GT demonstrate that the GT effect was more pronounced when the transformed cloud cover was <–1. Because an original cloud cover value of zero corresponds to clear sky over the grid point, we further discuss the effects of GT on clear days in Section 4.2.

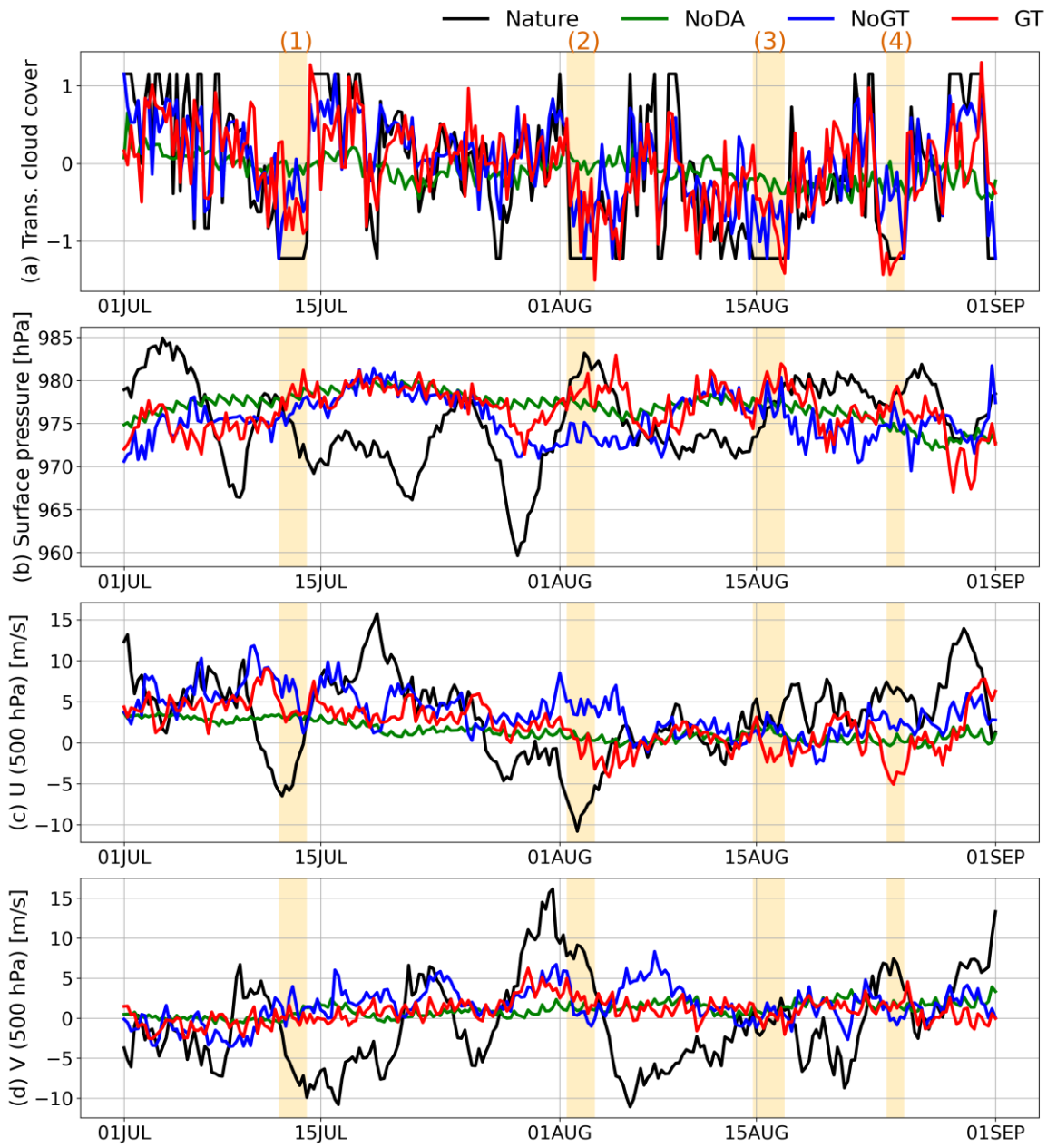

Figure 6. Time series of data assimilation results at a single grid point on Honshu Island, Japan (see Figure 2) for (a) transformed cloud cover, (b) surface pressure, (c) 500 hPa zonal wind, and (d) 500 hPa meridional wind. Black lines indicate results of the "nature" run. Green, blue, and red lines indicate simulation results for NoDA, NoGT, and GT, respectively. Yellow shading indicates > 30 h periods during which Gaussian-transformed cloud cover was continuously < –1.

4 Discussion

4.1 Effects of GT on rainfall and downward solar radiation

Here we discuss the results for rainfall and downward solar radiation (DSR), which exhibit significant non-Gaussianity (e.g., Lien *et al*., 2013) similar to cloud cover. We conducted an additional experiment, "GT_new," which assimilated transformed cloud cover as in GT, with GT rainfall and DSR in the first guess background field. The rainfall and DSR results obtained in the three experiments (NoGT, GT, and GT_new) are shown in Figure 7.

The 2-month RMSE reduction from NoDA for rainfall is shown in Figures 7. The rainfall field in NoGT deteriorated near 40°N compared to the control experiment. GT reduced regional RMSE by 2.47% over Japan compared to NoGT (RMSE reduction increased from 5.37% to 7.84%). GT improvements were mainly distributed over Tohoku, Japan. When we also applied GT rainfall in the first guess, its RMSE improved over the whole target area, and the regional RMSE was improved by 25.11% compared to the original GT experiment (regional averaged RMSE reduction increased from 7.84% to 32.95%). Figure S4 shows a scatterplot of the original 6 h rainfall in the nature run and RMSE reductions in the GT_new experiment, relative to NoGT. A negative correlation was detected between the nature values and the RMSE reduction. The larger improvements obtained for smaller rainfall values suggest that GT worked better for zero precipitation. It was more difficult to reproduce rainy days through total cloud cover assimilation, possibly due to uncertainties in the vertical cloud distribution.

The DSR results are shown in Figures 7d–f. Original cloud cover assimilation improved the DSR field mainly over land areas north of 40°N, with a regional RMSE reduction of 0.56%. GT of cloud cover had little effect in improving DSR estimation. GT results remained negative around a range of 30°–35°N. Figure 7f shows the results of GT_new, which applied Gaussian-transformed DSR in the first guess. Except in northern Korea, the Shikoku region of Japan, and some ocean regions, DSR was improved in most areas and RMSE was reduced by 2.28% over Japan compared to GT (regional averaged RMSE reduction increased from 2.57% to 4.85%).

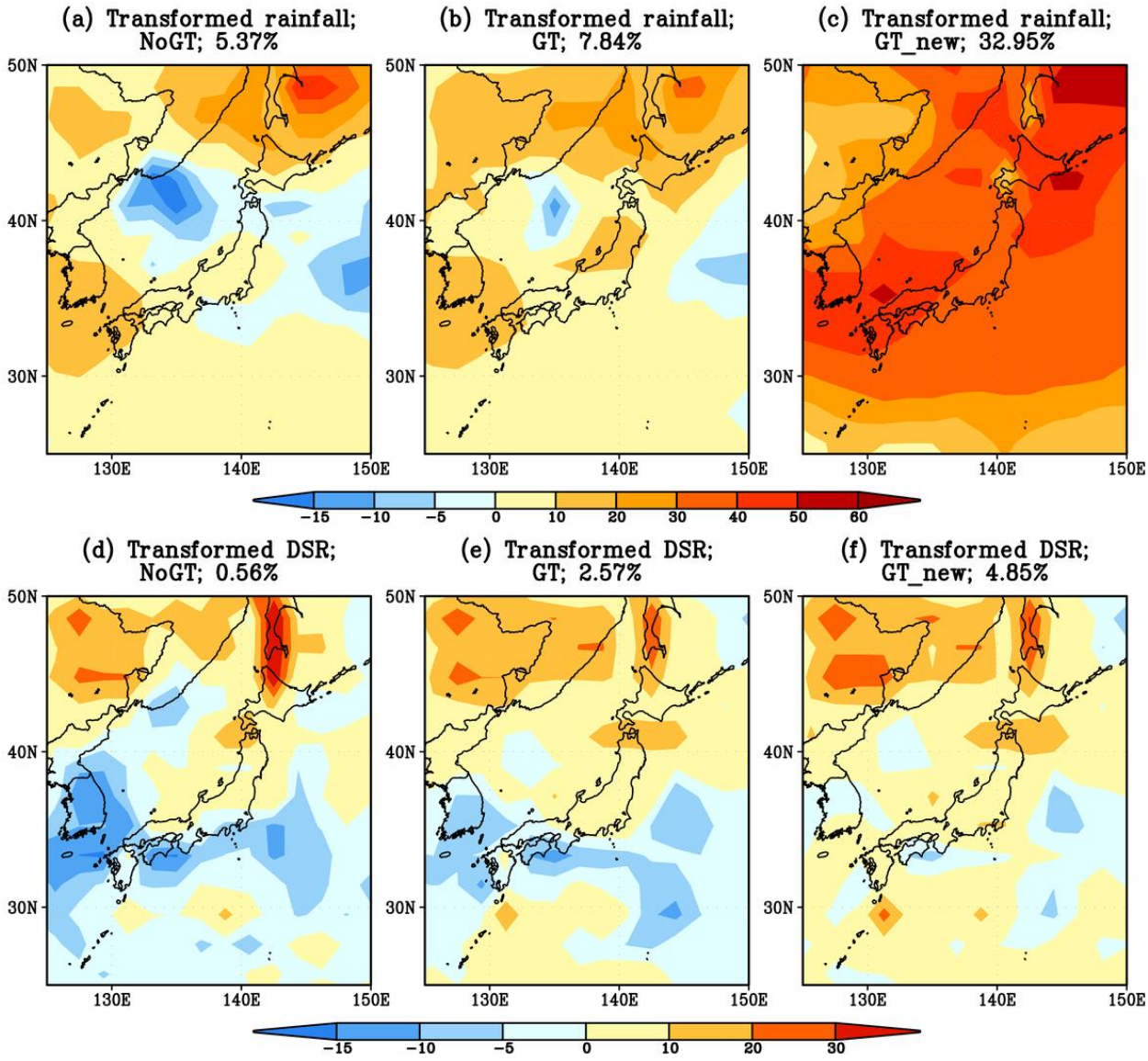

Figure 7. Horizontal distributions of 2-month RMSE reductions of (a, b, c) rainfall and (d, e, f) downward solar radiation (DSR) for (a, d) NoGT, (b, e) GT, and (c, f) GT_new relative to NoDA. All results were Gaussian transformed for consistency. Percentages are regional averages. Positive values indicate improvement relative to NoDA.

Lien *et al*. (2013) directly assimilated Gaussian-transformed precipitation and showed that the 11-month averaged RMSE of zonal wind was reduced by 37% globally by precipitation GT when using relatively large observational errors. Although assimilating rainfall observations recorded in diaries before the 19th century was challenging, our results demonstrate that we were able to improve non-normally distributed variables (e.g., rainfall

and DSR) by applying GT to the first guess of the cloud cover assimilation process. In particular, GT of the rainfall first guess fields showed RMSE improvements of >30% due to the high non-Gaussianity of rainfall distribution. It should be noted that in reconstructing actual rainfall that occurred before modern instrumental records, an inverse transformation method must be applied to the transformed field, as performed by Kotsuki *et al*. (2017).

4.2 GT impact at a geopotential height of 500 hPa

The 2-month temporal variation in regional averaged RMSE reduction by NoGT and GT is shown in Figure 8. GT had the greatest effects on rainfall due to its highly non-Gaussian characteristics (Figure 8h). Overall, GT contributed to RMSE reductions in all variables and reduced the variability of RMSE reductions, as shown in the histogram distributions. Figure S5 shows that GT improved the regional averaged 2-month RMSE reductions of all variables.

Two periods were particularly noteworthy: July 28–31 and August 1–5 (red and yellow shading, Figure 8). Although performance varied among the eight variables, most showed similar behavior during these two periods. The clearest contrast was in surface pressure (Figure 8f): NoGT performed better than GT during July 28–31, whereas GT performed better than NoGT during August 1–5. Some other variables, such as meridional wind, specific humidity, and cloud cover, also exhibited contrasting performances between NoGT and GT during these two periods. We further analyzed geopotential height at 500 hPa to investigate the possible causes of these contrasts.

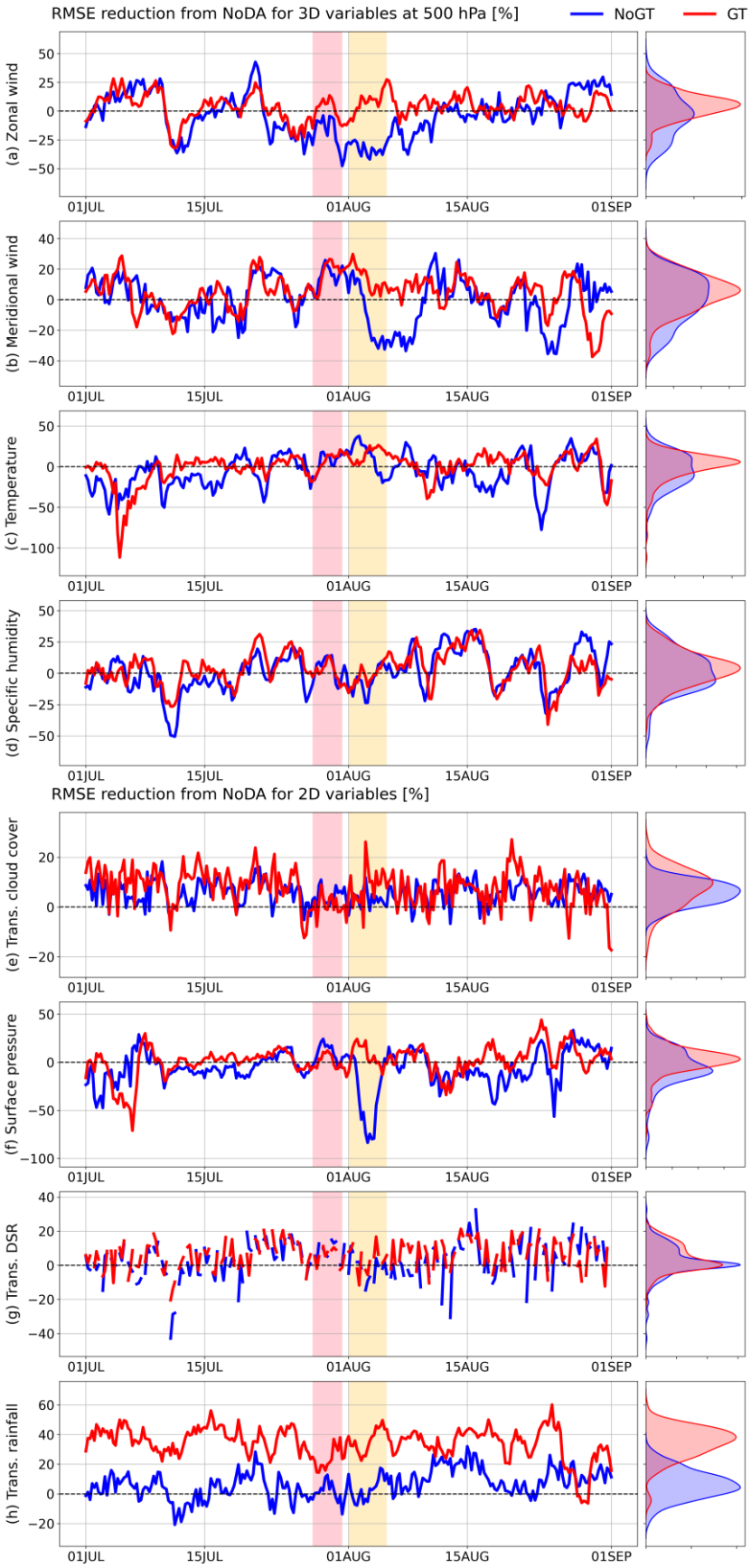

397

Figure 8. Time series of regional averaged RMSE reductions from NoDA. Blue and red lines indicate RMSE reductions for NoGT and GT, respectively. (a–d) Results of zonal wind, meridional wind, temperature, and specific humidity, respectively, at 500 hPa. (e–h) Results of cloud cover, surface pressure, DSR, and rainfall, respectively. GT results for DSR and rainfall are those of GT_new, with GT also performed in the model background covariance. Results in (e), (g), and (h) are Gaussian-transformed values for consistency. Histogram distributions of each atmospheric variable are presented to the right of each figure. Two periods of interest, July 27–31 and August 1–5, are indicated by red and yellow shading.

Figure 9 shows the large-scale horizontal distribution of a geopotential height of 500 hPa on two dates. This geopotential height was higher over Japan than over the surrounding region on August 4, 2017 but not on July 28, 2017. These height patterns were consistent during July 28–31 and August 1–5, respectively (Figure S6). Therefore, based on the results shown in Figures 8 and 9, we hypothesize that cloud cover GT had more pronounced impacts when the 500 hPa geopotential height in nature was higher near Japan than in other regions.

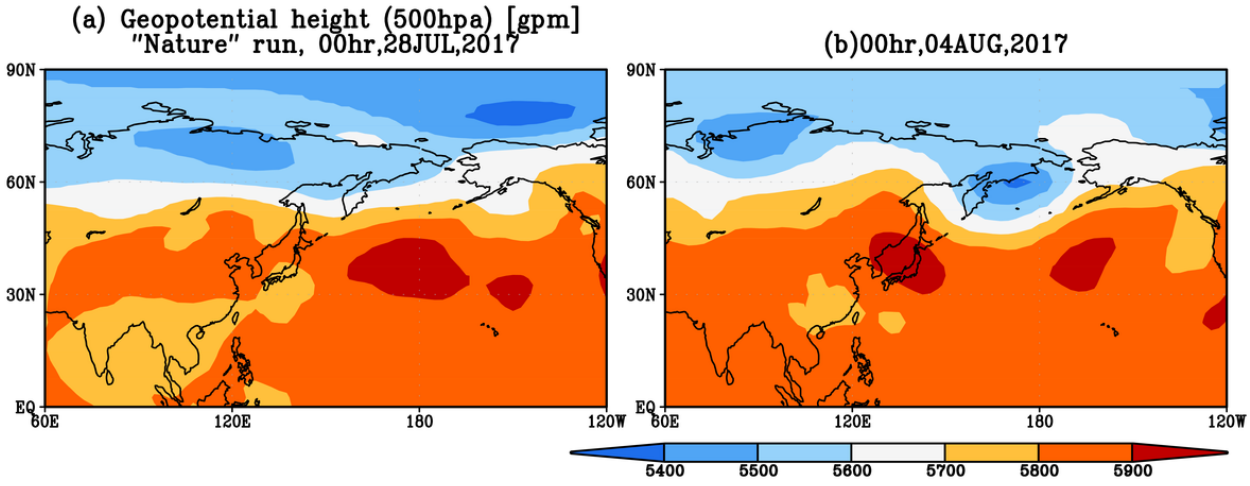

Figure 9. Horizontal distributions of 500 hPa geopotential height for the “nature” run on (a) July 28 and (b) August 4, 2017.

To further verify this hypothesis, we examined a 2-month time series of the nature run values and RMSE differences for a geopotential height of 500 hPa (Figure 10). When geopotential height showed a marked upward trend, as in early July and early August, RMSE

differences between NoGT and GT (calculated as RMSE_NoGT – RMSE_GT) were positive. Figure 10c shows a scatter plot of these two quantities, indicating a positive correlation between 500 hPa geopotential height and RMSE differences (r = 0.52). This phenomenon may have been caused by the enhanced GT impact when 500 hPa geopotential height was higher in nature, i.e., when the weather near grid points in Japan was clear, with low total cloud cover.

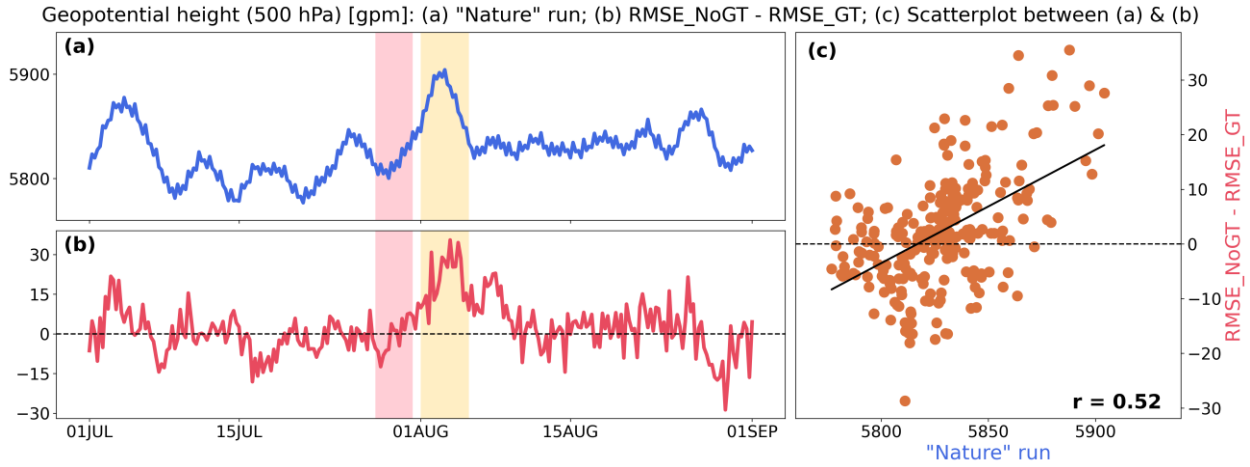

Figure 10. Time series of (a) regional averaged 500 hPa geopotential height in the "nature" run and (b) regional averaged RMSE differences between NoGT and GT (RMSE_NoGT–RMSE_GT). Red and yellow shading are as in Figure 8. (c) Scatterplot of the results shown in (a) and (b); r is the correlation coefficient.

Previous studies have focused on evaluating data assimilation performance in reconstructing 500 hPa geopotential height, particularly in historical climatology studies (e.g., Steiger *et al*., 2017). By contrast, we applied OSSE framework to demonstrate the role of 500 hPa geopotential height in cloud cover assimilation, and showed that GT effects were more pronounced when 500 hPa geopotential height was higher over Japan.

5 Summary and Conclusions

We conducted OSSEs to investigate the impacts of GT in cloud cover data assimilation for diary-based historical weather reconstruction. A control experiment without observations (NoDA) and two experiments assimilating cloud cover (NoGT and GT) were

performed over Japan.

Compared to NoGT, the 2-month RMSE of zonal wind, meridional wind, air temperature, and specific humidity were improved by 8.7%, 5.1%, 4.2%, and 1.4%, respectively, in the mid-troposphere by GT of cloud cover. For two-dimensional variables, 2-month RMSE of cloud cover, surface pressure, rainfall, and downward solar radiation are improved by 2.2%, 5.2%, 31.0%, and 4.3% over Japan, respectively. We also obtained improvements by applying GT to first guess values in the assimilation process for non-normally distributed variables (e.g., rainfall and DSR). The GT impact appeared to be more pronounced when the weather near Japan was clear, with low total cloud cover. We demonstrated that 500 hPa geopotential height over Japan was positively correlated with the GT impact.

For the reconstruction of actual rainfall that occurred before modern instrumental records, an inverse transformation method must be applied to the transformed field; this can be achieved using an observation-based empirical function (e.g., Kotsuki *et al*., 2017). The treatment of categorized diary data also requires consideration (Brázdil *et al*., 2010). Despite these practical limitations, the increasing availability and reliability of documentary records (e.g., Brázdil *et al*., 2005; Camenisch *et al*., 2019; White *et al*., 2018) suggests that GT could play an important role in the high-resolution reconstruction of historical weather.

Acknowledgments

This work was supported by JRPs-LEAD with DFG, Japan Society for the Promotion of Science (JSPS) KAKENHI Grant 18H03794 and 16H06291, the Integrated Research Program for Advancing Climate Models (TOUGOU) Grant Number JPMXD0717935457, ArCS II (Program Grant Number JPMXD1420318865), and DIAS from the Ministry of Education, Culture, Sports, Science and Technology (MEXT), Japan. KT was supported by JSPS KAKENHI Grant 19J01337. The authors gratefully thank Dr. Wenchao Ma, Mr. Haimao Lan, and Dr. Gaohong Yin for discussions and suggestions.

Data Availability Statement

The experiment results in this study are available online

472 (http://doi.org/10.5281/zenodo.4722443).

473

474 **References**

475 Alpert, J. C., Kanamitsu, M., Caplan, P. M., Sela, J. G., White, G. H., & Kalnay, E. (1988).
476 Mountain induced gravity wave drag parameterization in the NMC medium-range
477 forecast model. *Preprints of the Eighth Conference on Numerical Weather Prediction*
478 (pp. 726–733). Baltimore, MD: American Meteorological Society.

479 Bishop, C. H., Etherton, B. J., & Majumdar, S. J. (2001). Adaptive sampling with the
480 ensemble transform Kalman filter Part I: Theoretical aspects. *Monthly Weather Review*,
481 *129*(3), 420–436. https://doi.org/10.1175/1520-
482 0493(2001)129<0420:ASWTET>2.0.CO;2

483 Bocquet, M., Pires, C. A., & Wu, L. (2010). Beyond gaussian statistical modeling in
484 geophysical data assimilation. *Monthly Weather Review*, *138*(8), 2997–3023.
485 https://doi.org/10.1175/2010MWR3164.1

486 Brázdil, R., Dobrovolný, P., Luterbacher, J., Moberg, A., Pfister, C., Wheeler, D., & Zorita,
487 E. (2010). European climate of the past 500 years: new challenges for historical
488 climatology. *Climatic Change*, *101*(1–2), 7–40. https://doi.org/10.1007/s10584-009-
489 9783-z

490 BráZdil, R., Pfister, C., Wanner, H., Storch, H. Von, & Luterbacher, J. (2005). Historical
491 Climatology In Europe – The State Of The Art. *Climatic Change*, *70*(3), 363–430.
492 https://doi.org/10.1007/s10584-005-5924-1

493 Brázdil, R., Valášek, H., Chromá, K., Dolák, L., Řezníčková, L., Bělínová, M., et al. (2019).
494 The climate in south-east Moravia, Czech Republic, 1803–1830, based on daily weather
495 records kept by the Reverend Šimon Hausner. *Climate of the Past*, *15*(4), 1205–1222.
496 https://doi.org/10.5194/cp-15-1205-2019

497 Brönnimann, S., Franke, J., Breitenmoser, P., Hakim, G., Goosse, H., Widmann, M., et al.
498 (2013). Transient state estimation in paleoclimatology using data assimilation. *PAGES*
499 *News*, *21*(2), 74–75. https://doi.org/10.22498/pages.21.2.74

Camenisch, C., Bauch, M., Huhtamaa, H., Pei, Q., & White, S. (2019). Climate Reconstruction and Impacts from the Archives of Societies. *Past Global Changes Magazine*, *27*(2), 22498. https://doi.org/10.22498/pages.27.2.73

Camenisch, C., White, S., Pei, Q., & Huhtamaa, H. (2020). Editorial: Recent results and new perspectives in historical climatology: An overview. *Past Global Changes Magazine*, *28*(2), 2020. https://doi.org/10.22498/pages.28.2.35

Chen, F., Yuan, Y., Wei, W., Yu, S., Zhang, T., Shang, H., et al. (2015). Tree-ring recorded hydroclimatic change in Tienshan mountains during the past 500 years. *Quaternary International*, *358*, 35–41. https://doi.org/10.1016/j.quaint.2014.09.057

Chou, M.-D. (1992). A Solar Radiation Model for Use in Climate Studies. *Journal of the Atmospheric Sciences*, *49*(9), 762–772. https://doi.org/10.1175/1520-0469(1992)049<0762:ASRMFU>2.0.CO;2

Chou, M.-D., & Suarez, M. J. (1994). An efficient thermal infrared radiation parameterization for use in general circulation models. *Nasa Tech. Memo*, *104606*(3), 85. Retrieved from http://citeseerx.ist.psu.edu/viewdoc/summary?doi=10.1.1.26.4850

Chu, G., Sun, Q., Wang, X., Liu, M., Lin, Y., Xie, M., et al. (2012). Seasonal temperature variability during the past 1600 years recorded in historical documents and varved lake sediment profiles from northeastern China. *The Holocene*, *22*(7), 785–792. https://doi.org/10.1177/0959683611430413

Compo, G. P., Whitaker, J. S., Sardeshmukh, P. D., Matsui, N., Allan, R. J., Yin, X., et al. (2011). The Twentieth Century Reanalysis Project. *Quarterly Journal of the Royal Meteorological Society*, *137*(654), 1–28. https://doi.org/10.1002/qj.776

Domínguez-Castro, F., Gallego, M. C., Vaquero, J. M., Herrera, R. G., Peña-Gallardo, M., El Kenawy, A., & Vicente-Serrano, S. M. (2019). Twelve Years of Daily Weather Descriptions in North America in the Eighteenth Century (Mexico City, 1775–86). *Bulletin of the American Meteorological Society*, *100*(8), 1531–1547. https://doi.org/10.1175/BAMS-D-18-0236.1

Ek, M. B., Mitchell, K. E., Lin, Y., Rogers, E., Grunmann, P., Koren, V., et al. (2003). Implementation of Noah land surface model advances in the National Centers for Environmental Prediction operational mesoscale Eta model. *Journal of Geophysical*

Research: Atmospheres, *108*(D22), 2002JD003296. https://doi.org/10.1029/2002JD003296

Evensen, G. (1994). Sequential data assimilation with a nonlinear quasi-geostrophic model using Monte Carlo methods to forecast error statistics. *Journal of Geophysical Research*, *99*(C5). https://doi.org/10.1029/94jc00572

Evensen, G. (2003). The Ensemble Kalman Filter: theoretical formulation and practical implementation. *Ocean Dynamics*, *53*(4), 343–367. https://doi.org/10.1007/s10236-003-0036-9

Franke, J., González-Rouco, J. F., Frank, D., & Graham, N. E. (2011). 200 years of European temperature variability: insights from and tests of the proxy surrogate reconstruction analog method. *Climate Dynamics*, *37*(1–2), 133–150. https://doi.org/10.1007/s00382-010-0802-6

Goosse, H., Crespin, E., de Montety, A., Mann, M. E., Renssen, H., & Timmermann, A. (2010). Reconstructing surface temperature changes over the past 600 years using climate model simulations with data assimilation. *Journal of Geophysical Research*, *115*(D9), D09108. https://doi.org/10.1029/2009JD012737

Hakim, G. J., Emile-Geay, J., Steig, E. J., Noone, D., Anderson, D. M., Tardif, R., et al. (2016). The last millennium climate reanalysis project: Framework and first results. *Journal of Geophysical Research: Atmospheres*, *121*(12), 6745–6764. https://doi.org/10.1002/2016JD024751

Hunt, B. R., Kostelich, E. J., & Szunyogh, I. (2007). Efficient data assimilation for spatiotemporal chaos: A local ensemble transform Kalman filter. *Physica D: Nonlinear Phenomena*, *230*(1–2), 112–126. https://doi.org/10.1016/j.physd.2006.11.008

Kanamitsu, M., Kumar, A., Juang, H.-M. H., Schemm, J.-K., Wang, W., Yang, F., et al. (2002). NCEP Dynamical Seasonal Forecast System 2000. *Bulletin of the American Meteorological Society*, *83*(7), 1019–1037. https://doi.org/10.1175/1520-0477(2002)083<1019:NDSFS>2.3.CO;2

Kotsuki, S., Miyoshi, T., Terasaki, K., Lien, G.-Y., & Kalnay, E. (2017). Assimilating the global satellite mapping of precipitation data with the Nonhydrostatic Icosahedral

559 Atmospheric Model (NICAM). *Journal of Geophysical Research: Atmospheres*, *122*(2),
560 631–650. https://doi.org/10.1002/2016JD025355

561 Lien, G.-Y., Kalnay, E., & Miyoshi, T. (2013). Effective assimilation of global precipitation:
562 simulation experiments. *Tellus A: Dynamic Meteorology and Oceanography*, *65*(1),
563 19915. https://doi.org/10.3402/tellusa.v65i0.19915

564 McDermott, F. (2004). Palaeo-climate reconstruction from stable isotope variations in
565 speleothems: a review. *Quaternary Science Reviews*, *23*(7–8), 901–918.
566 https://doi.org/10.1016/j.quascirev.2003.06.021

567 McElwain, L., & Sweeney, J., (2007). *Key Meteorological Indicators of Climate Change in*
568 *Ireland*. Johnstown Castle, Wexford, Ireland: Environmental Protection Agency.

569 Mikami, T. (2008). Climatic variations in Japan reconstructed from historical documents.
570 *Weather*, *63*(7), 190–193. https://doi.org/10.1002/wea.281

571 Miyoshi, T. (2011). The Gaussian Approach to Adaptive Covariance Inflation and Its
572 Implementation with the Local Ensemble Transform Kalman Filter. *Monthly Weather*
573 *Review*, *139*(5), 1519–1535. https://doi.org/10.1175/2010MWR3570.1

574 Mock, C. J. (1991). Historical evidence of a cold, dry summer during 1849 in the
575 northeastern Great Basin and adjacent Rocky Mountains. *Climatic Change*, *18*(1), 37–
576 66. https://doi.org/10.1007/BF00142504

577 Moorthi, S., & Suarez, M. J. (1992). Relaxed Arakawa-Schubert. A Parameterization of
578 Moist Convection for General Circulation Models. *Monthly Weather Review*, *120*(6),
579 978–1002. https://doi.org/10.1175/1520-0493(1992)120<0978:RASAPO>2.0.CO;2

580 Nash, D., Adamson, G., Ashcroft, L., Bauch, M., Camenisch, C., Degroot, D., et al. (2020).
581 Climate indices in historical climate reconstructions: A global state-of-the-art. *Climate*
582 *of The Past Discussions*, 1–48. https://doi.org/10.5194/cp-2020-126

583 Orszag, S. A. (1970). Transform Method for the Calculation of Vector-Coupled Sums:
584 Application to the Spectral Form of the Vorticity Equation. *Journal of the Atmospheric*
585 *Sciences*, *27*(6), 890–895. https://doi.org/10.1175/1520-
586 0469(1970)027<0890:TMFTCO>2.0.CO;2

Ott, E., Hunt, B. R., Szunyogh, I., Zimin, A. V., Kostelich, E. J., Corazza, M., et al. (2004). A local ensemble Kalman filter for atmospheric data assimilation. *Tellus A: Dynamic Meteorology and Oceanography*, *56*(5), 415–428. https://doi.org/10.3402/tellusa.v56i5.14462

Pfister, C., Camenisch, C., & Dobrovolný, P. (2018). Analysis and interpretation: temperature and precipitation indices. In *The Palgrave Handbook of Climate History* (pp. 115-129). London: Palgrave Macmillan.

Pfister, L., Brönnimann, S., Schwander, M., Isotta, F. A., Horton, P., & Rohr, C. (2020). Statistical reconstruction of daily precipitation and temperature fields in Switzerland back to 1864. *Climate of the Past*, *16*(2), 663–678. https://doi.org/10.5194/cp-16-663-2020

Pfister, L., Hupfer, F., Brugnara, Y., Munz, L., Villiger, L., Meyer, L., et al. (2019). Early instrumental meteorological measurements in Switzerland. *Climate of the Past*, *15*(4), 1345–1361. https://doi.org/10.5194/cp-15-1345-2019

Proctor, C. J., Baker, A., Barnes, W. L., & Gilmour, M. A. (2000). A thousand year speleothem proxy record of North Atlantic climate from Scotland. *Climate Dynamics*, *16*(10–11), 815–820. https://doi.org/10.1007/s003820000077

Shao, X. (2005). Reconstruction of precipitation variation from tree rings in recent 1000 years in Delingha, Qinghai. *Science in China Series D*, *48*(7), 939. https://doi.org/10.1360/03yd0146

Slivinski, L. C., Compo, G. P., Whitaker, J. S., Sardeshmukh, P. D., Giese, B. S., McColl, C., et al. (2019). Towards a more reliable historical reanalysis: Improvements for version 3 of the Twentieth Century Reanalysis system. *Quarterly Journal of the Royal Meteorological Society*, *145*(724), 2876–2908. https://doi.org/10.1002/qj.3598

Steiger, N. J., Hakim, G. J., Steig, E. J., Battisti, D. S., & Roe, G. H. (2014). Assimilation of Time-Averaged Pseudoproxies for Climate Reconstruction. *Journal of Climate*, *27*(1), 426–441. https://doi.org/10.1175/JCLI-D-12-00693.1

Steiger, N. J., Steig, E. J., Dee, S. G., Roe, G. H., & Hakim, G. J. (2017). Climate reconstruction using data assimilation of water isotope ratios from ice cores. *Journal of*

Geophysical Research: Atmospheres, *122*(3), 1545–1568. https://doi.org/10.1002/2016JD026011

Striberger, J., Björck, S., Ingolfsson, O., Kjaer, K. H., Snowball, I., & Uvo, C. B. (2011). Climate variability and glacial processes in eastern Iceland during the past 700 years based on varved lake sediments. *Boreas*, *40*(1), 28–45. https://doi.org/10.1111/j.1502-3885.2010.00153.x

Thomas, E. K., & Briner, J. P. (2009). Climate of the past millennium inferred from varved proglacial lake sediments on northeast Baffin Island, Arctic Canada. *Journal of Paleolimnology*, *41*(1), 209–224. https://doi.org/10.1007/s10933-008-9258-7

Toride, K., Neluwala, P., Kim, H., & Yoshimura, K. (2017). Feasibility Study of the Reconstruction of Historical Weather with Data Assimilation. *Monthly Weather Review*, *145*(9), 3563–3580. https://doi.org/10.1175/MWR-D-16-0288.1

Tsuyuki, T., & Miyoshi, T. (2007). Recent Progress of Data Assimilation Methods in Meteorology. *Journal of the Meteorological Society of Japan. Ser. II*, *85B*, 331–361. https://doi.org/10.2151/jmsj.85B.331

Wackernagel, H. 2003. *Multivariate Geostatistics: an introduction with applications* (3rd ed.). Berlin: Springer.

Walsh, R. P. D., Glaser, R., & Militzer, S. (1999). The climate of Madras during the eighteenth century. *International Journal of Climatology*, *19*(9), 1025–1047. https://doi.org/10.1002/(SICI)1097-0088(199907)19:9<1025::AID-JOC402>3.0.CO;2-F

Whitaker, J. S., & Hamill, T. M. (2012). Evaluating Methods to Account for System Errors in Ensemble Data Assimilation. *Monthly Weather Review*, *140*(9), 3078–3089. https://doi.org/10.1175/MWR-D-11-00276.1

White, S., Pfister, C., & Mauelshagen, F. (Eds.). (2018). *The Palgrave handbook of climate history*. London: Palgrave Macmillan.

Yoshimura, M. (2007). An introduction to historical weather database in Japan (in Japanese). *Tenki*, 54, 191–194.

Zhang, S. Q., Zupanski, M., Hou, A. Y., Lin, X., & Cheung, S. H. (2013). Assimilation of Precipitation-Affected Radiances in a Cloud-Resolving WRF Ensemble Data

Assimilation System. *Monthly Weather Review*, *141*(2), 754–772. https://doi.org/10.1175/MWR-D-12-00055.1

Zhang, X.-Z., Ge, Q.-S., Fang, X.-Q., Zheng, J.-Y., & Fei, J. (2013). Precipitation variations in Beijing during 1860-1897 AD revealed by daily weather records from the Weng Tong-He Diary. *International Journal of Climatology*, *33*(3), 568–576. https://doi.org/10.1002/joc.3448

Zhu, H., Zheng, Y., Shao, X., Liu, X., Xu, Y., & Liang, E. (2008). Millennial temperature reconstruction based on tree-ring widths of Qilian juniper from Wulan, Qinghai Province, China. *Science Bulletin*, *53*(24), 3914–3920. https://doi.org/10.1007/s11434-008-0400-8

Monthly Weather Review

Supporting Information for

Impact of Gaussian Transformation on Cloud Cover Data Assimilation for Historical Weather Reconstruction

Xiaoxing Wang[1], Kinya Toride[2,3], and Kei Yoshimura[2,4]

[1] Graduate School of Frontier Sciences, The University of Tokyo, Kashiwa, Chiba, Japan

[2] Institute of Industrial Science, The University of Tokyo, Kashiwa, Chiba, Japan

[3] Department of Atmospheric Sciences, University of Washington, Seattle, WA, USA

[4] Earth Observation Research Center, Japan Aerospace Exploration Agency, Japan

Contents of this file

Text S1 to S2
Figures S1 to S6

Introduction

In the supporting text, we describe in detail the determination of ensemble member size (Text S1, Figure S1) and the covariance inflation method (Text S2, Figure S2) in local ensemble transform Kalman filter (LETKF). The Gaussian transformation (GT) impacts on clear days are shown in Figures S3, S4, and S6, and the 2-month RMSE reductions for all variables are summarized in Figure S5.

Text S1. LETKF ensemble size

We conducted pre-experiments using ensemble member sizes ranging from 20 to 90. Figure S1 shows RMSE reductions for NoGT and GT at different ensemble member sizes. Cloud cover improved as ensemble member size increased (Figure S1a). For other surface variables, 40 and 60 ensembles showed better performance (gray bars in other cases indicate negative reductions). Although differences between GT and NoGT were greater at an ensemble size of 40, the GT results were negative for both temperature and specific humidity (Figures S1d and S1e). Therefore, we adopted an ensemble member size of 60 in this study.

Text S2. LETKF covariance inflation method

We explored different covariance inflation method choices in LETKF. Figure S2 shows the vertical distribution of RMSE reductions by GT using no covariance inflation, adaptive covariance inflation (Miyoshi, 2011), and a relaxation-to-prior-spread (RTPS) scheme (α = 0.5) (Whitaker & Hamill, 2012). Zonal wind was markedly improved by RTPS in the mid-troposphere and below, compared to adaptive inflation and no inflation (Figure S2a). Differences among the three methods were clearest in meridional wind (Figure S2b). RTPS greatly improved the meridional wind field at all heights compared to the no inflation and adaptive inflation results. Air temperature (Figure S2c) and specific humidity (Figure S2d) showed similar results. RTPS generally showed better performance at <300 hPa. Therefore, we adopted RTPS (α = 0.5) as the covariance inflation method in this study.

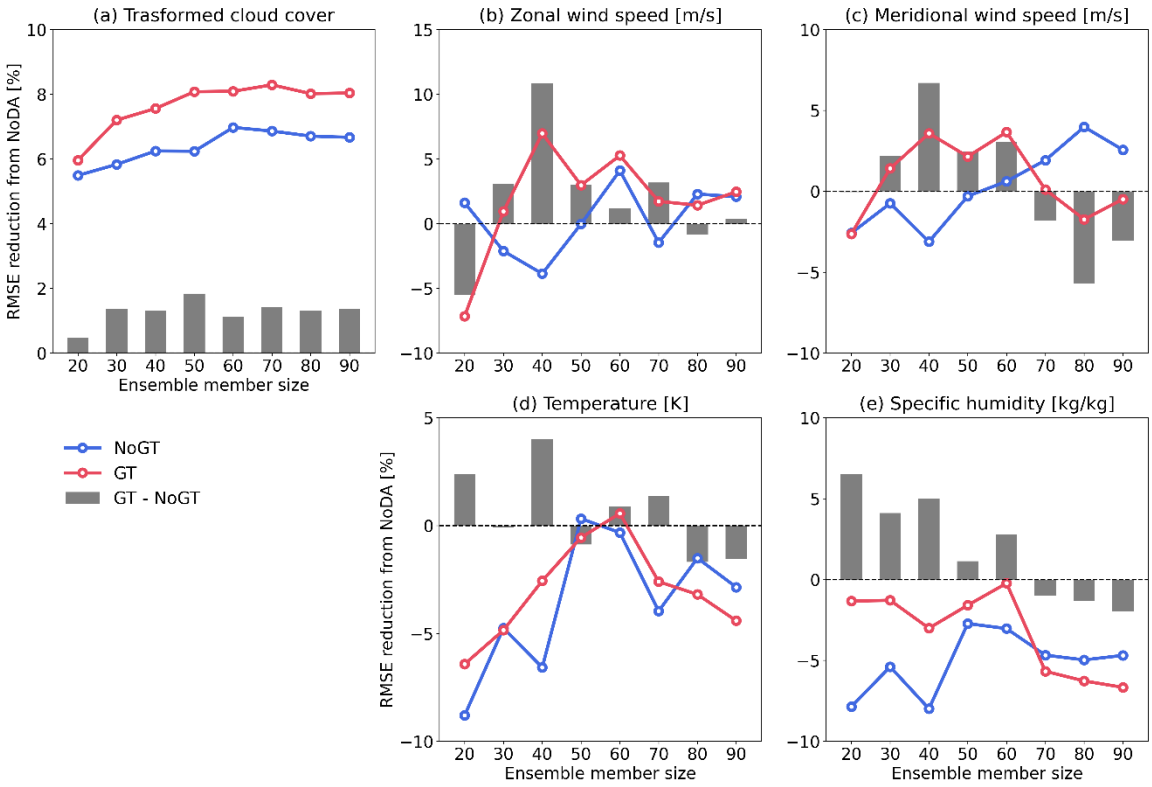

Figure S1. Regional averaged 2-month RMSE reductions of (a) cloud cover, (b) zonal wind, (c) meridional wind, (d) temperature, and (e) specific humidity for different ensemble member sizes. (b–e) Results near the surface. Blue and red lines show RMSE reductions from NoDA by NoGT and GT, respectively. Gray bars indicate differences between the red and blue lines. Positive values indicate improvement due to GT.

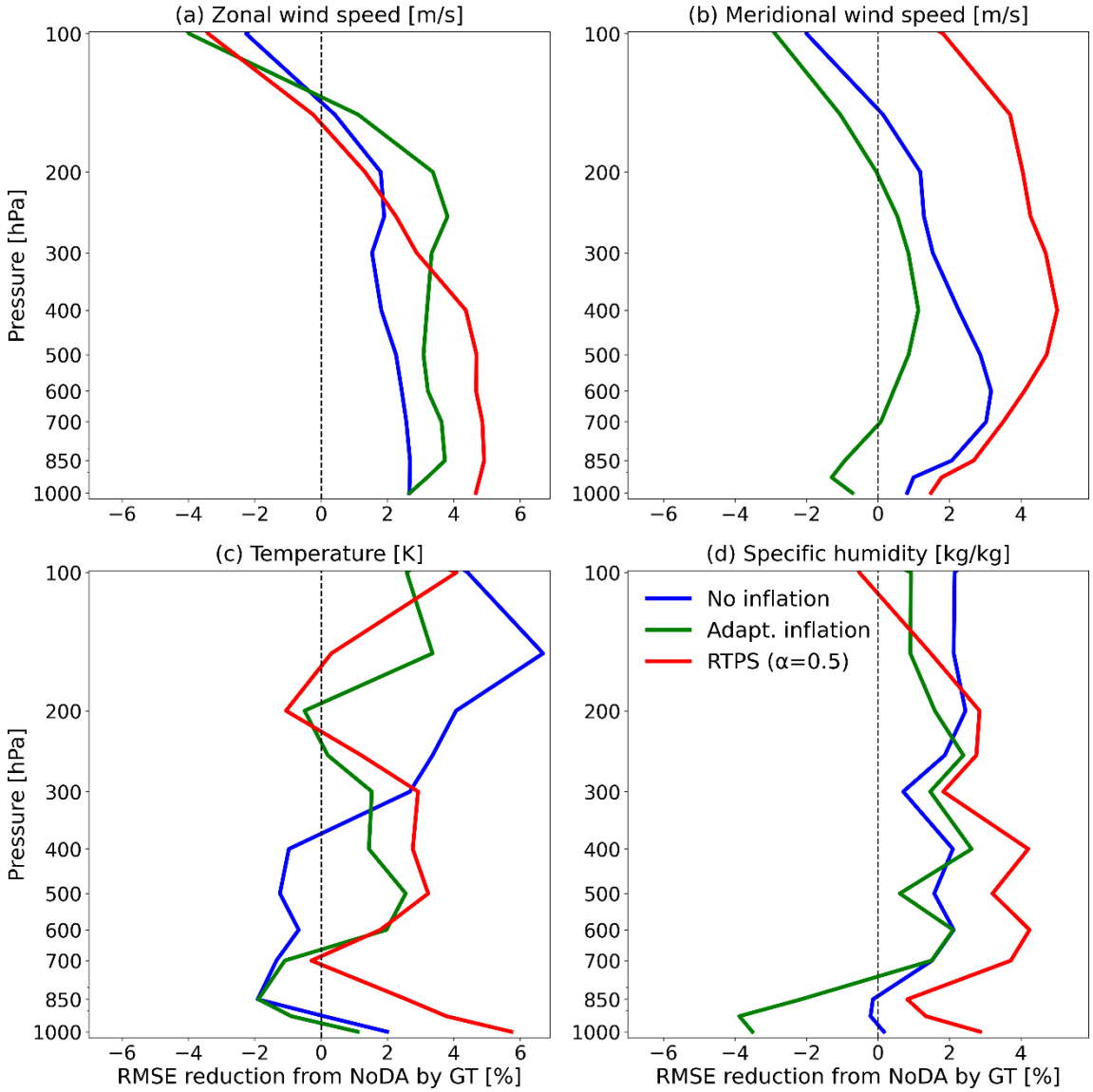

Figure S2. Vertical distributions of 2-month RMSE reductions due to GT relative to NoDA. Blue, green, and red lines indicate no covariance inflation, adaptive covariance inflation, and a relaxation-to-prior-spread method (α = 0.5). Results are regional averages of (a) zonal wind, (b) meridional wind, (c) temperature, and (d) specific humidity. Positive values indicate improvement relative to NoDA.

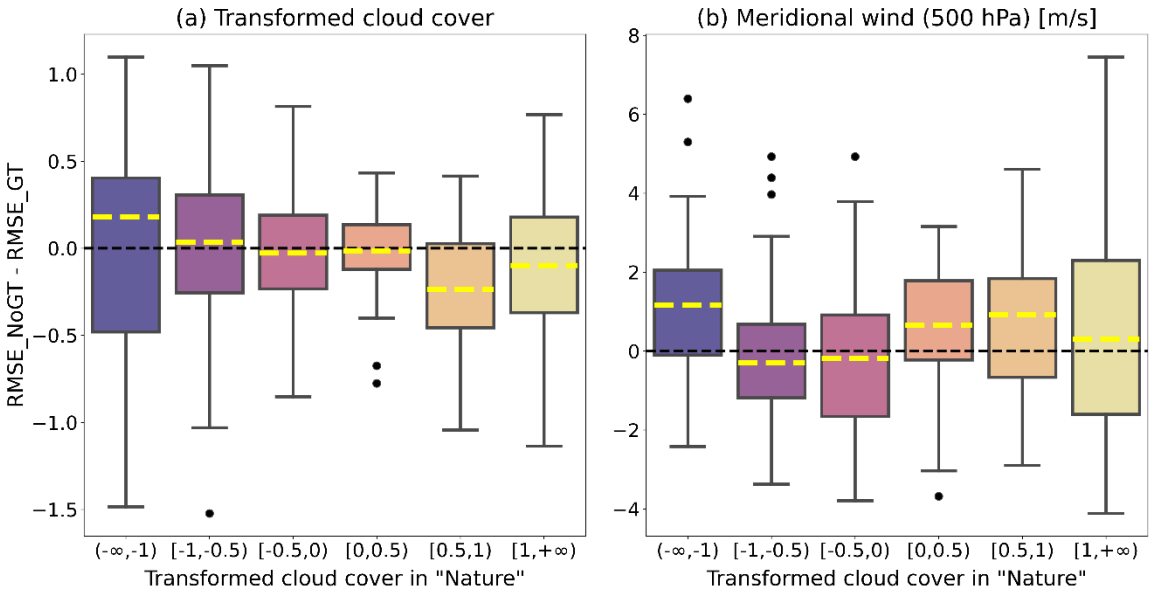

Figure S3. Boxplot grouped by transformed cloud cover for the “nature” run. Vertical axes are RMSE differences between NoGT and GT (RMSE_NoGT–RMSE_GT) at a single grid point on Honshu Island, Japan (see Figure 2) for (a) transformed cloud cover and (b) 500 hPa meridional wind. Yellow dashed lines in each box indicate median values. Positive values indicate improvement due to GT.

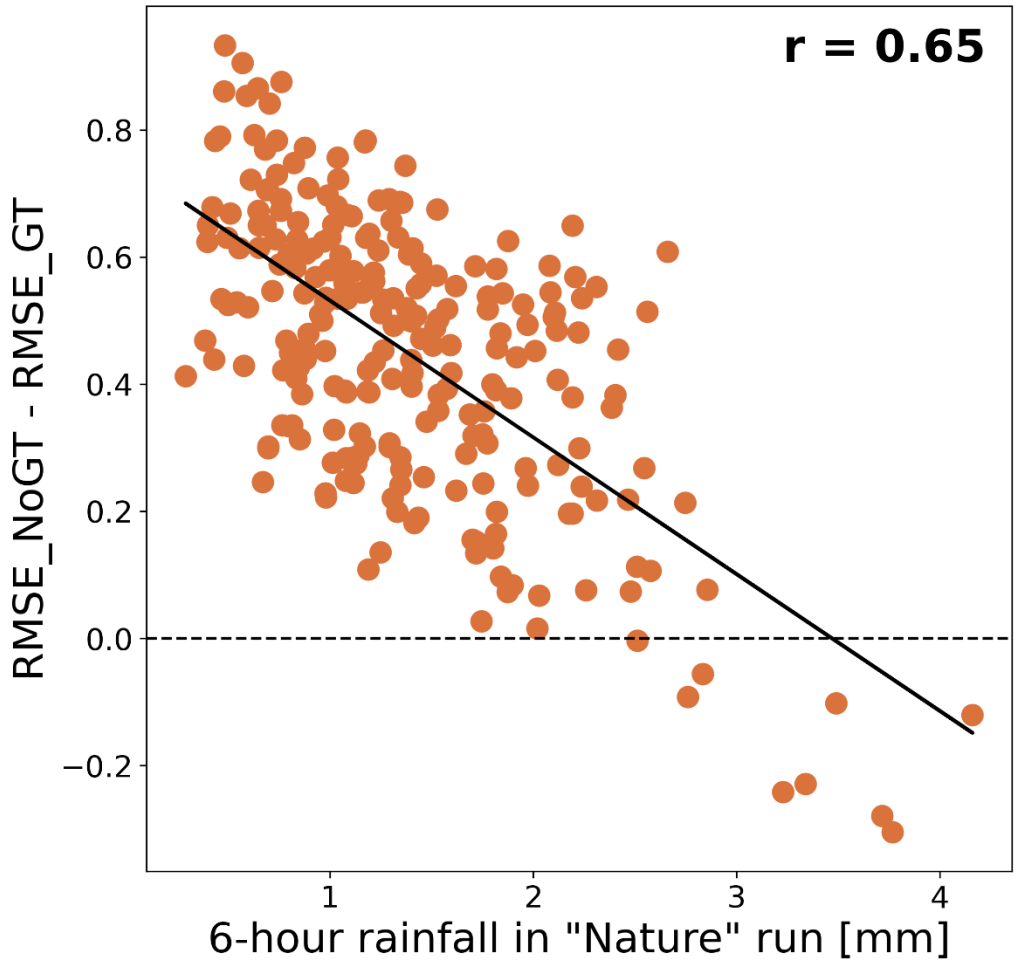

Figure S4. Scatterplot of original 6 h rainfall in the “nature” run and regional averaged rainfall RMSE differences between NoGT and GT (RMSE_NoGT–RMSE_GT). RMSE was calculated using Gaussian-transformed values. Positive values indicate improvement due to GT; r is the correlation coefficient.

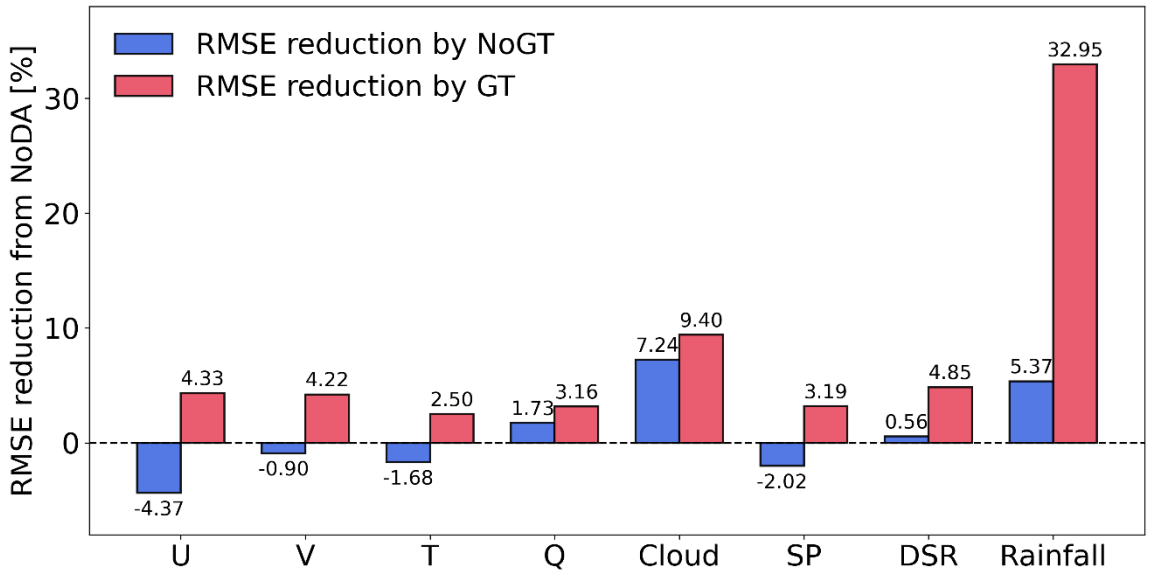

Figure S5. Summary of 2-month RMSE reductions from NoDA. Blue and red bars show RMSE reductions by NoGT and GT, respectively. U, V, T, and Q are three-dimensional variable results at 500 hPa, i.e., zonal wind, meridional wind, temperature, and specific humidity, respectively. Cloud, SP, DSR, and rainfall are two-dimensional variables, i.e., cloud cover, surface pressure, downward solar radiation, and rainfall, respectively. GT results for DSR and rainfall are GT_new results. Cloud, DSR, and rainfall results were Gaussian-transformed for consistency.

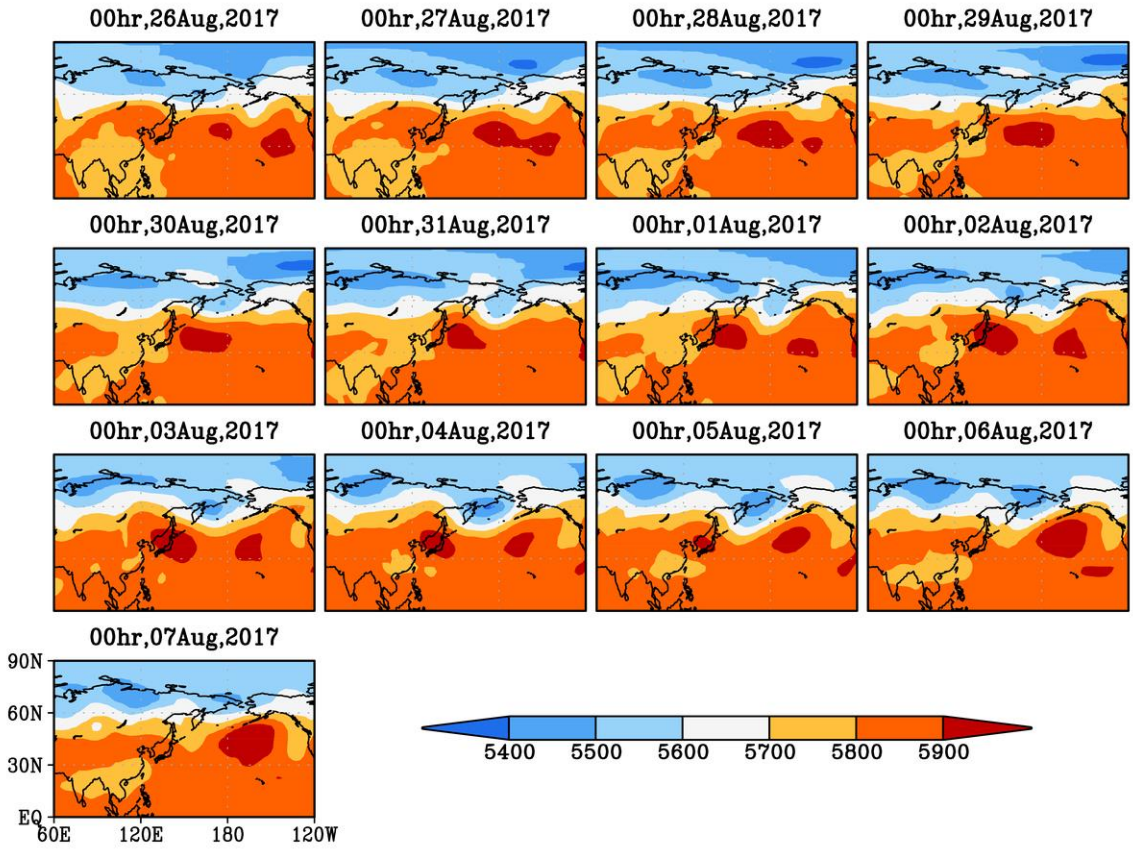

Figure S6. Horizontal distributions of 500 hPa geopotential height in the "nature" run during July 26–August 7, at 1-day intervals.